

# Sensitisation and Evolution of Chromium-depleted Zones in Fe–Cr–Ni–C Systems

T. SOURMAIL, C. H. TOO and H. K. D. H. BHADESHIA

Department of Materials Science and Metallurgy, University of Cambridge, Pembroke Street, Cambridge CB2 3QZ, UK.

(Received on February 27, 2003; accepted in final form on May 27, 2003)

The development of chromium concentration profiles in austenitic stainless steels, due to the grain boundary precipitation of carbides has been modelled, taking account of multicomponent effects, both in the estimation of the state of equilibrium at the carbide/matrix interface and in diffusion. A comparison against published experimental data shows that the theory accounts for the development of the depleted zone as well as self-healing, unlike recent work where these effects are treated as separate phenomena. At the same time, the present model preserves local equilibrium at the precipitate–matrix interface and provides a natural explanation for the observation of delays in reaching the minimum chromium content.

KEY WORDS: Cr-depleted zone; Cr profile;  $M_{23}C_6$ ; sensitisation; stainless steels.

## 1. Introduction

Austenitic stainless steels have many applications in industry for their corrosion resistance and weldability. However, carbide precipitation induced by the welding process or heat treatment can cause chromium-depletion near the grain boundaries, leading to a phenomenon known as sensitisation, in which the depleted zones become the focus of intense corrosion. Any model for sensitisation must therefore deal with carbide formation at grain boundaries in order to define the chromium-depleted zone. One of the difficulties in modelling the growth rate of the carbides in a multicomponent system such as a typical stainless steel, is that the solutes have different diffusivities, and yet must reach the precipitate at a rate compatible with the expected composition of the precipitate<sup>1,2)</sup>:

$$J_i = v(c_i^{\beta\gamma} - c_i^{\gamma\beta}) \quad \forall i \dots\dots\dots(1)$$

where  $J$  is the flux, the subscript  $i$  refers to the solute element,  $v$  is the interface velocity,  $c_i^{\beta\gamma}$  is the concentration of element in the precipitate ( $\beta$ ) phase in equilibrium with the matrix ( $\gamma$ ). This is henceforth referred to as the flux-balance condition.

In steels, the interstitial-diffusion of carbon is much faster than that of substitutional elements. It is therefore reasonable to assume<sup>3–6)</sup> that the activity of carbon in the matrix becomes uniform, *i.e.*, the activity at the carbide–matrix interface equals far away from the interface. This is illustrated in **Fig. 1**. Such models predict a minimum chromium concentration in the matrix at the carbide–matrix interface,  $c_{Cr(\min)}^{\gamma\beta}$  reached at the beginning of precipitation ( $t=0$ ). As precipitation progresses, the activity of carbon decreases and  $c_{Cr}^{\gamma\beta}$  increases as required by local equilibrium at the carbide–matrix interface.

Models by Stawström and Hillert,<sup>3)</sup> Was and Kruger,<sup>4)</sup>

and Bruemmer<sup>6)</sup> have applied this concept. With the restriction of a constant nickel content, Stawström and Hillert used a simple equation to calculate the carbon activity as a function of chromium and carbon. Was and Kruger introduced a more elaborate thermodynamic approach, accounting for Fe, Cr, Ni, C while Bruemmer added an empirical term to include the effect of Mo.

In these models, a knowledge of carbon isoactivity was used to determine the chromium concentration at the interface. Assuming a planar precipitate–matrix interface, the growth rate was then estimated by solving the diffusion equation ahead of the interface. It is worth noting that all of these models only allow for chromium modification when estimating the carbide–matrix interface composition. This is not strictly correct in systems with more than three components such as the one dealt with by Was and Kruger, and Bruemmer, since, for example there is no guarantee that the flux balance equations:

$$J_{Cr} = v(c_{Cr}^{\beta\gamma} - c_{Cr}^{\gamma\beta}) \dots\dots\dots(2)$$

$$J_{Ni} = v(c_{Ni}^{\beta\gamma} - c_{Ni}^{\gamma\beta}) \dots\dots\dots(3)$$

will be verified simultaneously for a unique velocity  $v$ .

As mentioned earlier, previous models<sup>3–6)</sup> implied that the  $c_{Cr(\min)}^{\gamma\beta}$  is reached at  $t=0$ . However, measurements<sup>7)</sup> indicate that  $c_{Cr}^{\gamma\beta}$  will only reach a minimum after a finite time  $\tau$  as in **Fig. 2**.

Sahlaoui *et al.*<sup>8)</sup> recently developed a different approach based on Mayo<sup>9)</sup> where the process is divided into two. Chromium-depletion is considered to occur during the growth of the carbide according to an empirical equation:

$$c_{Cr}^{\gamma\beta} = \bar{c}_{Cr}^{\gamma} \exp\left(-k \frac{t}{\tau}\right) \dots\dots\dots(4)$$

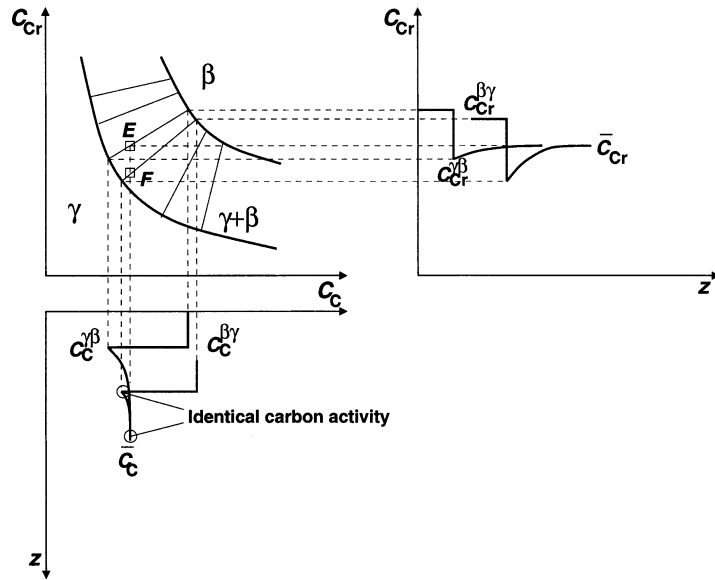


Fig. 1. Diagram showing the flux-balance tie-line (passes through F) and the mass-balance tie-line (passes through E). The subscripts refer to the elements and z is the distance. Note that carbon isoactivity is not identical with isoconcentration due to the gradient of chromium.

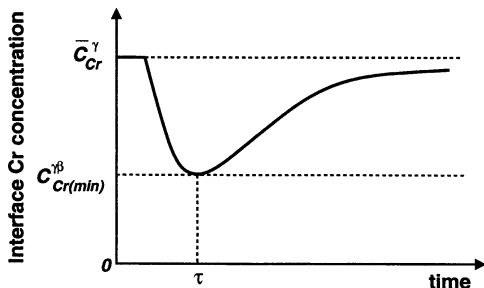


Fig. 2. Typical carbide-matrix interface chromium concentration curve.  $\bar{c}_{Cr}^{\gamma}$  is the bulk chromium concentration.

where  $\tau$  is time to reach minimum  $c_{Cr}^{\gamma/beta}$ ,  $t$  is time and  $k$  is a constant. Following precipitation, there is a tendency for the homogenisation of gradients, a phenomenon described as self-healing; it was assumed that self-healing is a second stage, due to chromium diffusion alone, after carbide growth is completed.

The agreement achieved with experimental data by Sahlaoui *et al.*'s model is essentially due to a fitting parameter  $\tau$  in the first stage of the calculation. Furthermore, the use of a two-stage description violates the reasonable assumption that the carbide-matrix interface should remain in local equilibrium during diffusion-controlled growth. It will become evident later in this paper that the predicted values of  $c_{Cr}^{\gamma/beta}$  should underestimate experimental measurements which suffer from spatial resolution problems. In the present work we hope to show that the experimental data can be explained in a unified model consistent with thermodynamic equilibrium.

2. Numerical Model for Diffusion

2.1. The Diffusion Equation

To account for the multicomponent nature of the diffusion ahead of the interface, the fluxes were expressed as<sup>10)</sup>:

$$J_i^L = -c_i M_i \nabla \mu_i \dots \dots \dots (5)$$

where  $J_i^L$  is the flux of element  $i$  in the lattice fixed f.o.r. (frame of reference),  $c_i$  the concentration of element  $i$ ,  $M_i$  its mobility and  $\mu_i$  its chemical potential.

The mobilities were calculated as a function of the composition, as suggested by Ågren and Åkermark.<sup>11,12)</sup> Practical calculations are made in the volume-fixed f.o.r. (for example, Kirkaldy and Young<sup>13)</sup>), defined so that  $\sum_i V_i J_i^V = 0$  where  $V_i$  is the molar volume of component  $i$  and  $J_i^V$  the flux of component  $i$  through a surface of fixed coordinate in the volume-fixed f.o.r. Noting that:

$$J_i^V = J_i^L + c_i u \dots \dots \dots (6)$$

where  $u$  is the velocity of the lattice-fixed f.o.r. in the flux-fixed f.o.r., one obtains:

$$J_i^V = \sum_k^N \left( \delta_{ik} - x_i \frac{V_k}{V_m} \right) c_k M_k \nabla \mu_k \dots \dots \dots (7)$$

where  $N$  is the number of components in the system,  $V_m$  the molar volume of austenite ( $\sum_S x_i V_i$  where  $S$  refers to the substitutional elements), and  $x_i$  is the mole fraction of component  $i$  (note:  $c_i = x_i / V_m$ ). The evolution of the concentration with time is therefore governed by the following equation:

$$\frac{\partial x_i}{\partial t} = \nabla \sum_k \left( \delta_{ik} - x_i \frac{V_k}{V_m} \right) x_k M_k \nabla \mu_k \dots \dots \dots (8)$$

which is re-written:

$$\frac{\partial x_i}{\partial t} = \nabla \sum_k A_{ik} \nabla \mu_k \dots \dots \dots (9)$$

with

$$A_{ik} = \left( \delta_{ik} - x_i \frac{V_k}{V_m} \right) x_k M_k$$

for convenience. It is assumed that growth occurs at a pla-

**Table 1.** Bulk and interface compositions at 700°C, under different conditions: in the first case (I), isoactivity is obtained by modification of the interface Cr content, but the Ni content is fixed.

Conditions	Phase	Cr	Ni	C×10 <sup>2</sup>	Velocity / m s <sup>-1</sup>
Bulk	γ	0.1962	0.0823	0.276	-
Mass balance equilibrium	γ	0.19	0.083	0.021	-
	M <sub>23</sub> C <sub>6</sub>	0.69	6.7×10 <sup>-6</sup>	20.69	-
Interface composition I	γ	0.047	0.081	0.216	2.7×10 <sup>-12</sup>
	M <sub>23</sub> C <sub>6</sub>	0.482	0.008	20.69	-
Interface composition II	γ	0.048	0.131	0.163	3.1×10 <sup>-12</sup>
	M <sub>23</sub> C <sub>6</sub>	0.492	0.012	20.69	-

nar interface, reducing the problem to one dimension, with diffusion occurring perpendicular to the grain boundary.

**2.2. Finite Difference Model**

In the following, the first superscript (*j*) refers to the node, while the second (*n*) refers to the time step.

Using central difference for space and forward difference for time, the following finite-difference equivalent for Eq. (9) is obtained:

$$\frac{x_i^{j,n+1} - x_i^{j,n}}{\Delta t} = \frac{1}{(\Delta X)^2} \sum_k [A_{ik}^{j+1/2,n} (\mu_k^{j+1,n} - \mu_k^{j,n}) - A_{ik}^{j-1/2,n} (\mu_k^{j,n} - \mu_k^{j-1,n})] \dots\dots\dots(10)$$

or re-arranging:

$$x_i^{j,n+1} = x_i^{j,n} + \frac{\Delta t}{(\Delta X)^2} \sum_k [A_{ik}^{j+1/2,n} (\mu_k^{j+1,n} - \mu_k^{j,n}) - A_{ik}^{j-1/2,n} (\mu_k^{j,n} - \mu_k^{j-1,n})] \dots\dots\dots(11)$$

where Δ*t* is the time step and Δ*X* the grid spacing. The values *A<sub>ik</sub><sup>j+1/2,n</sup>* and *A<sub>ik</sub><sup>j-1/2,n</sup>* can be defined using:

$$A_{ik}^{j+1/2,n} = \frac{1}{2} [A_{ik}^{j,n} + A_{ik}^{j+1,n}] \dots\dots\dots(12)$$

**2.3. Implementation**

To evaluate Eq. (11), a computer program was interfaced with the thermodynamic software MT-DATA.<sup>14)</sup> At the beginning of each loop, the chemical potentials and *A<sub>ik</sub><sup>j,n</sup>* are calculated on each node given its composition. The composition of each node is then updated following Eq. (11). This method dispenses with computing the diffusion coefficients from the mobilities.

The boundary conditions were set as follow:

$$x_i^{j,0} = \bar{x}_i \quad \forall i, j \dots\dots\dots(13)$$

$$x_i^{n_{max},k} = \bar{x}_i \quad \forall i, j \dots\dots\dots(14)$$

that is to say, all compositions are set to the bulk composition  $\bar{x}_i$  at time *t*=0, and the composition remains equal to that of the bulk on the last node *n<sub>max</sub>*, furthest away from the precipitate. An ancillary node is used to apply the central difference on the last node. The boundary condition at the precipitate/matrix interface is discussed later.

**2.4. Composition at the Interface**

The composition at the interface between the precipitate growing on the grain boundary, whether it is M<sub>7</sub>C<sub>3</sub> or M<sub>23</sub>C<sub>6</sub>, has most of the time been considered to be under

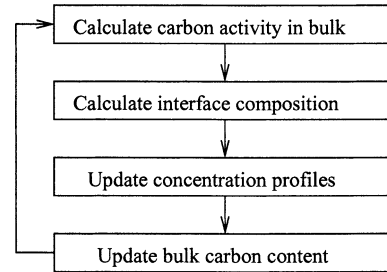


**Fig. 3.** Simplified functioning of the model. At each time step, the tie-line is calculated that satisfies the flux-balance for the present carbon activity, an iteration is then performed in the finite-difference model to update the concentration profiles ahead of the interface. From the increase in size of the precipitate, the amount of carbon removed from the bulk is calculated.

local equilibrium.<sup>3-6)</sup> However, this composition is, in general, not that given by the tie-line satisfying the mass-balance, but by that satisfying the flux-balance, that is the set of conditions:

$$J_i |_{\xi=0} = v (c_i^{\beta\gamma} - c_i^{\gamma\beta}) \dots\dots\dots(15)$$

where ξ is the distance away from the interface.

The complexity of the task means that most models so far have limited the search for the flux-balance to the Fe–Cr–C system (isoactivity of carbon). An algorithm which uses MT-DATA has been written to solve the problem in a general manner: not only is the isoactivity of carbon satisfied, but the solution also verifies the flux balance for other substitutional elements; for the example of a Fe–Cr–Ni–C system:

$$J_{Cr} |_{\xi=0} = v (c_{Cr}^{\beta\gamma} - c_{Cr}^{\gamma\beta}) \dots\dots\dots(16)$$

$$J_{Ni} |_{\xi=0} = v (c_{Ni}^{\beta\gamma} - c_{Ni}^{\gamma\beta}) \dots\dots\dots(17)$$

**Table 1** provides the results obtained under different assumptions. In the first case, only Cr is modified to obtain carbon isoactivity. Clearly, the interface Ni content being below that of the bulk is not consistent with growth of the precipitate, since the latter has a lower Ni content. The second calculation satisfies both the isoactivity of carbon and equality of the Cr and Ni fluxes.

Note that at the interface, the flux is estimated using a forward spatial difference as it is not possible to define an ancillary node as is done for the last node in the bulk.

**2.5. Overall Method**

The overall functioning of the model is illustrated in **Fig. 3**. Further technical details can be found, together with the source code for this model, on <http://www.msm.cam.ac.uk/map>

When considering the amount of carbon removed from the matrix by the growth of the precipitate, it is necessary to define a volume from which the carbon is drawn. Stawström and Hillert<sup>3)</sup> have used half the grain size for this purpose. This is discussed in detail later in the text.

### 3. Results and Discussion

#### 3.1. Interface Chromium Concentration

Predictions of the chromium concentration in the matrix at the carbide–matrix interface,  $c_{Cr}^{\gamma\beta}$ , have been made based on the composition of type 304 austenitic stainless steels as given in Table 2.

Figure 4 compares the calculated  $c_{Cr}^{\gamma\beta}$  as a function of temperature, against previous work. Earlier approaches by Stawström and Hillert,<sup>3)</sup> and Fullman<sup>15)</sup> over-predicted  $c_{Cr}^{\gamma\beta}$  at high temperatures. Bruemmer<sup>6)</sup> applied an empirical relation which was obtained by direct measurements of chromium-depletion. It is not therefore surprising that Bruemmer's model is in good agreement with the measured data and follow the trend of experimental data in which  $c_{Cr}^{\gamma\beta}$  increases with temperature.

Measurements of  $c_{Cr}^{\gamma\beta}$  were obtained using a scanning transmission electron microscope with an energy dispersive X-ray spectrometer (STEM-EDS) for which the beam spreading was estimated to be  $\approx 25$  nm.<sup>7)</sup>

It is argued here that measurements are likely to overestimate the actual interface composition for two reasons: as is shown later, strong concentration gradients are expected in the vicinity of the grain boundary, meaning that the averaging effect caused by the beam spreading is likely to have a significant influence on the result. Furthermore, the problem of having a grain boundary parallel to the beam is never mentioned in the experimental procedure, although having to satisfy both this condition and the tilt required by the detector geometry is certainly a source of experimental difficulties.

Table 2. Composition of type 304 austenitic stainless steel used in this example.

AISI type	Composition / wt%			
	Fe	Cr	Ni	C
304	72.71	18.48	8.75	0.06

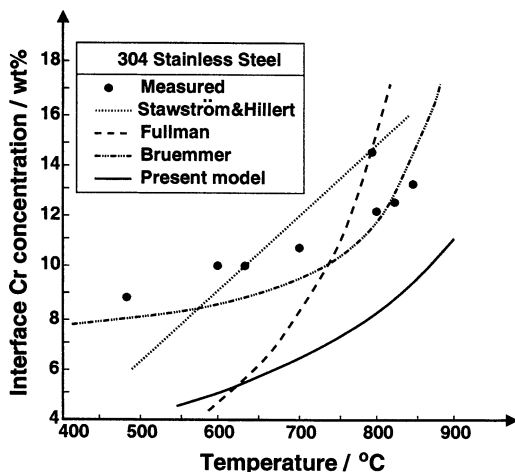


Fig. 4. Comparison of measured and predicted  $c_{Cr}^{\gamma\beta}$  values.

There are therefore good reasons to believe that the measured ‘interface’ composition is best compared with the average composition of the first  $\approx 25$  nm of material in contact with the grain boundary.

Figure 5 shows the evolution of the average weight fraction of chromium in the first 15, 20 and 25 nm, for a 18.48 Cr, 8.75 Ni, 0.06 C (wt%) steel aged at 700°C. The relatively small influence in the distance over which the average is calculated is to be expected. If on the contrary, a strong dependency had been shown over this range, the literature would surely provide significantly different measurements depending on the exact experimental conditions; this does not seem to be the case. In the discussion that follows, the interface value is referred to as  $c_{Cr,2}^{\gamma\beta}$  and the averaged value calculated over the first 25 nm as  $c_{Cr}^{\gamma\beta}$ .

#### 3.2. Self-healing and Soft-impingement

As demonstrated above, a delay in the chromium depletion can be explained by considering the average composition which is expected to be measured rather than the exact interface composition predicted.

The self-healing process, on the other hand, is due to the shift of the tie-line towards the mass-balance equilibrium as the precipitation progresses, as illustrated in Fig. 6. The time scale in which this phenomenon occurs is strongly dependent on the volume ( $V=Sd$ ) from which carbon is withdrawn.  $S$  is set to be a unit area, and  $d$  is the distance ahead

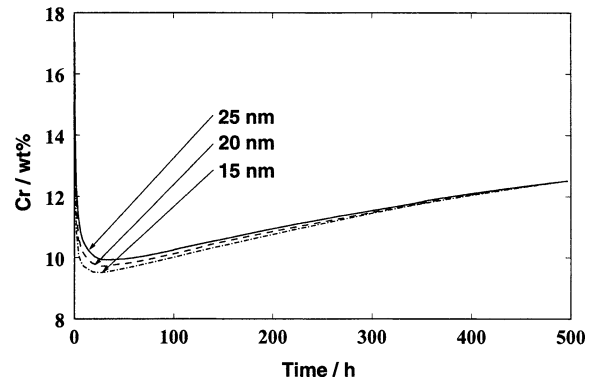


Fig. 5. Calculated average weight percent of chromium in the first 15, 20 and 25 nm, for a 18.48 Cr, 8.75 Ni, 0.06 C (wt%) steel aged at 700°C.

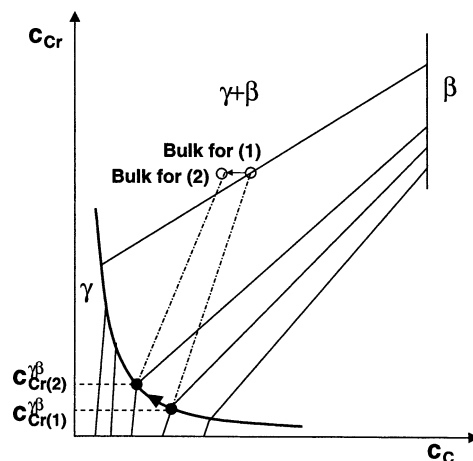


Fig. 6. Schematic phase diagram showing the change of  $c_{Cr}^{\gamma\beta}$  during precipitation.

of the grain boundary from which carbon can be drawn. For a small  $d$ , the carbon concentration is expected to drop rapidly and self-healing should start relatively early (Fig. 7).

At the limit where the distance  $d$  is infinite, the activity of carbon in the bulk is constant and self-healing never occurs. For very small  $d$ , sensitisation can be avoided as the increase of Cr concentration at the interface is fast enough so that the average in the first 25 nm never drops below a critical value. This has been observed experimentally by Beltran *et al.*<sup>16)</sup>: with a grain size of 15  $\mu\text{m}$ , sensitisation was found to be virtually reduced to zero throughout the ageing while a far greater effect is observed for a grain size of 150  $\mu\text{m}$ . The relation between  $d$  and the grain size, overlooked in many previous works, is discussed later.

The evolution of the carbon mole fraction in the bulk is calculated according to:

$$\bar{x}_C(t+\Delta t) = \left( \frac{\bar{x}_C(t)}{V_m^\gamma} Sd - Sv(t)\Delta t \frac{(x_C^{\beta\gamma} - x_C^{\gamma\beta})}{V_m^\beta} \right) \frac{V_m^\gamma}{d} \dots (18)$$

where  $S$  is the surface area taken to be a unit area,  $d$  the distance from which carbon can be withdrawn,  $\bar{x}_C(t)$  the mole fraction of carbon in the bulk at time  $t$ , and  $v(t)$  the velocity of the precipitate interface at time  $t$ .

Figure 8(a) shows predicted chromium concentration profiles ahead of the grain boundary for identical temperatures and ageing durations, for a variety of values of  $d$ . In all cases, the interface chromium mole fraction at  $t=0$

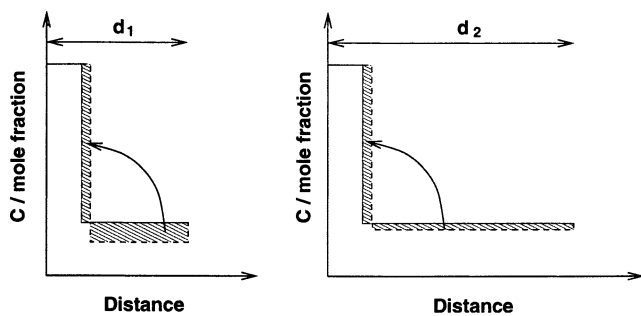


Fig. 7. Schematic illustration showing the dependency of the rate of carbon depletion on the distance available for withdrawing carbon. If an infinite distance is available from which to draw carbon, the activity of the latter is constant with time and the Cr concentration at the interface never changes, meaning there is no self-healing.

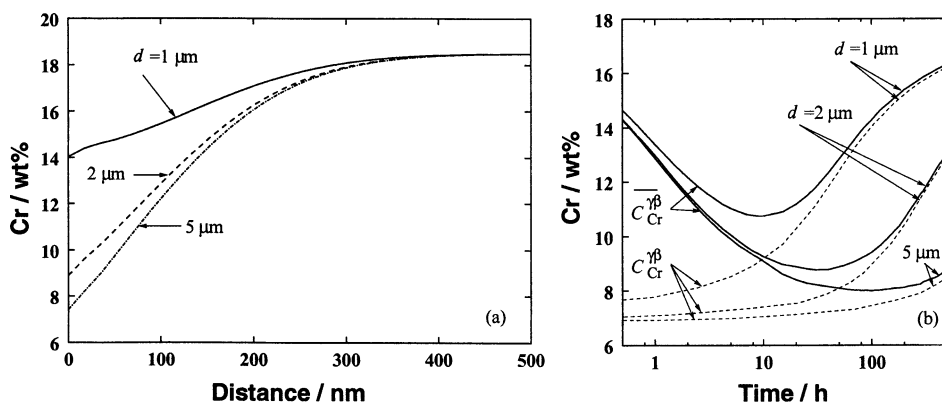


Fig. 8. Effect of  $d$  on the evolution of the Cr concentration profile ahead of the grain boundary.

is identical. After 100 h, significant tie-line shifting has occurred for the smallest  $d$  but virtually none for the largest  $d$ . Figure 8(b) shows the average chromium mole fraction ( $\bar{c}_{Cr}^{\gamma\beta}$ ) over the first 25 nm in the different cases. Note that for a small value of  $d$ , the minimum of  $\bar{c}_{Cr}^{\gamma\beta}$  is about 4 wt% higher than the minimum interface value (at  $t=0$ ) while this difference is reduced to 1 wt% for  $d=5 \mu\text{m}$ .

### 3.3. Sensitisation and De-sensitisation: Comparison with Experiments

One of the difficulties occurring in physical models is to establish a correspondence between the predicted evolution of the concentrations and the sensitisation phenomenon itself. A criterion could be that sensitisation starts when  $\bar{x}_{Cr}^{\gamma\beta}$  is below a critical value, and ends when it raises above this value.

As illustrated in Fig. 8(b), the onset of sensitisation is relatively independent on  $d$ . Prediction of desensitisation is less successful (Fig. 9); possible reasons are discussed later.

### 3.4. The Significance of $d$

Stawström and Hillert<sup>3)</sup> have used half the grain size for  $d$ . However, the real soft-impingement being a three-dimension problem, it seems more appropriate to attribute to each calculation volume a sixth of the grain, given that, if a simple cubic model is used to represent a grain, six faces will actually draw carbon from the same volume.

If, as with Stawström and Hillert,<sup>3)</sup> a distance of 25  $\mu\text{m}$  is used, a film of about 0.2  $\mu\text{m}$  on each side of the boundary, is required to obtain the average 1% volume fraction of  $M_{23}C_6$  found in type 304 at 700°C. This is significantly larger than the typical 200 nm<sup>7)</sup> observed as a maximum thickness (meaning that the equivalent film of uniform thickness would be thinner).

In the present model, desensitisation times are still slightly overestimated even if  $d$  is set to a sixth of the grain size (Fig. 9).

All of the models for sensitisation,<sup>3,4,7-9)</sup> only consider grain-boundary precipitation, which always happen at the very early stage of ageing. This can be sufficient, as illustrated previously, to predict the onset of sensitisation. However, desensitisation occurs on longer time scale where other carbon sinks becomes active within the grain. In particular, Lewis and Hattersley<sup>17)</sup> reported observing intragranular  $M_{23}C_6$  as early as after 30 min at 750°C, after a few hundred hours, the quantity of intragranular  $M_{23}C_6$  is

significant (Fig. 10). The consequences may not be negligible in steels with relatively large grain sizes.

### 3.5. Influence of Intragranular Precipitation

To verify whether the shorter than predicted self-healing times could be attributed to intragranular precipitation, a simple modification was made to the existing model, under the following assumptions: intragranular particles of  $M_{23}C_6$  form on dislocations, on which nucleation is taken to be instantaneous. Note that this is not unreasonable given the identification of intragranular  $M_{23}C_6$  after 30 min at  $750^\circ\text{C}$ .<sup>17)</sup>

Assuming a spherical shape, the volume increment during a time step is given by:

$$\Delta V_{\text{intra}} = N4\pi r^2 dr \dots\dots\dots(19)$$

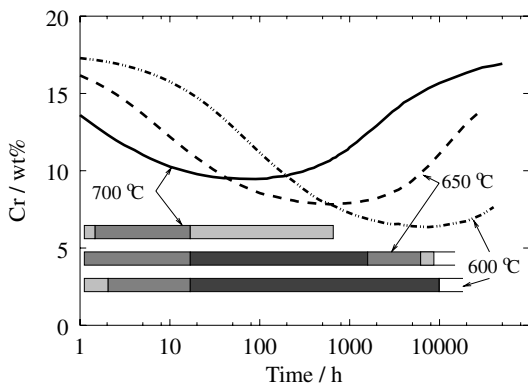


Fig. 9. Average Cr concentration near the interface (25 nm) calculated with the present model. Calculated with  $d=8.3 \mu\text{m}$  (grain size  $50 \mu\text{m}$ ).

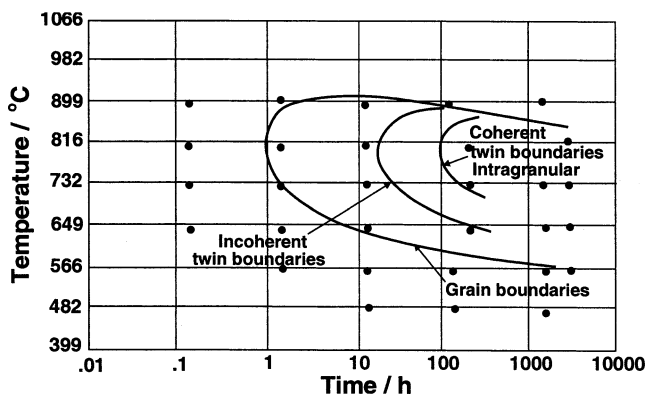


Fig. 10. Time-Temperature-Precipitation diagram for  $M_{23}C_6$  in 304 type austenitic stainless steel.

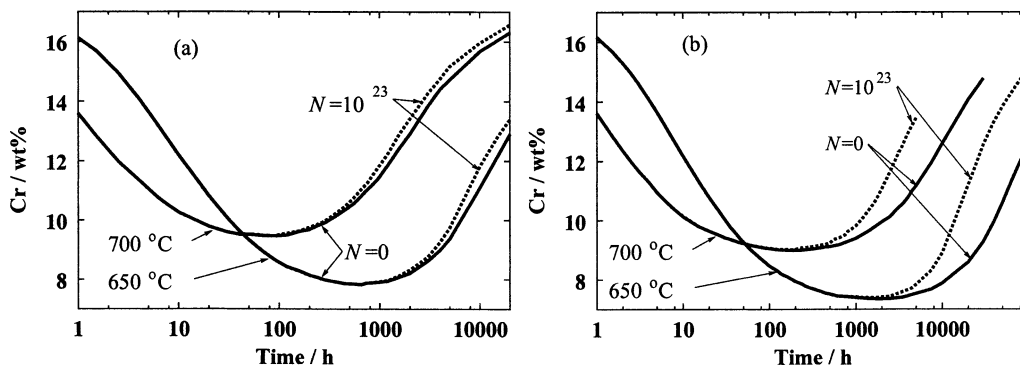


Fig. 12. Effect of intragranular precipitation on the evolution of  $\overline{c_{Cr}^{\gamma\beta}}$  at 650 and  $700^\circ\text{C}$  for a grain size of (a)  $50 \mu\text{m}$  and (b)  $150 \mu\text{m}$ .

where  $N$  is the number density of particles, given by  $N_v^{1/3}L_d$  where  $N_v$  is the number of atoms per unit volume and  $L_d$  the dislocation density.<sup>10)</sup>  $dr$  is estimated from the interface velocity. The corresponding amount of carbon is removed from the matrix at each time step. Figure 11 shows the evolution of  $\overline{c_{Cr}^{\gamma\beta}}$  in type 304 at  $650^\circ\text{C}$  for a grain size of  $50 \mu\text{m}$  ( $d=8.3 \mu\text{m}$ ), for different values of  $N$ . For values of  $N$  representative of an annealed material ( $N=10^{17}$  to  $N=10^{23} \text{m}^{-3}$ )<sup>18)</sup> the influence is small.

The role of intragranular precipitation is also dependent on the grain size, as illustrated in Fig. 12, which shows that, for  $N=10^{23} \text{m}^{-3}$ , the desensitisation time is significantly shifted to the left.

Figure 12 illustrates the estimated influence of intragranular precipitation on a material of two different grain sizes,  $50$  and  $150 \mu\text{m}$ , at  $650$  and  $700^\circ\text{C}$ . As is expected, precipitation within the grain has no influence on the onset of sensitisation but can strongly affect the predicted self-healing as the grain size increases and the amount of surface per unit volume is reduced.

### 4. Summary and Conclusions

The sensitisation of austenitic stainless steels occurs because of the chromium-depletion accompanying the precipitation alloy carbides; a model has been developed for the estimation the chromium concentration profile in the vicinity of austenite grain boundaries. This takes into account the multicomponent nature of austenitic stainless steels, assuming local equilibrium at the carbide/matrix interface.

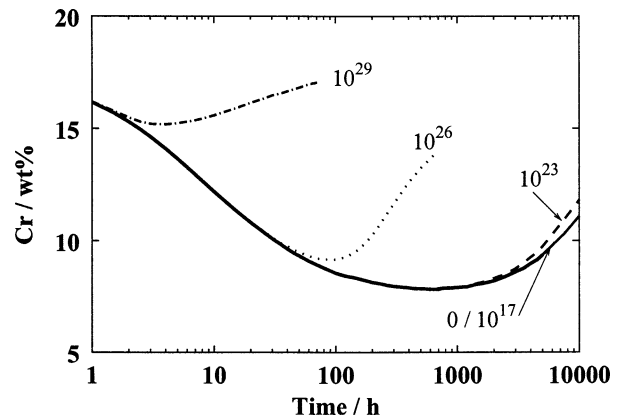


Fig. 11. Effect of intragranular precipitation on the evolution of  $\overline{c_{Cr}^{\gamma\beta}}$  at  $650^\circ\text{C}$ , for a grain size of  $50 \mu\text{m}$ , for different  $N$ . For  $N=10^{17}$  and  $N=10 \text{m}^{-3}$ , the curves are identical.

Predictions are found to be in good agreement with published literature data, once the extent of space over which the experimental data were determined, is taken into account.

It should be noted that, by contrast with many former approaches, there are here no fitting parameters (*e.g.* Ref. 8)), or modifications of the thermodynamics for  $M_{23}C_6$  formation (*e.g.* Ref. 6)), as the general SGTE database is used through MT-DATA. It is shown, first, that there is no need to modify these thermodynamic data to explain the measured Cr minimum, which, it is argued, should be under-predicted; and second, that the division of the sensitisation process in a two-stage process (*e.g.* Refs. 8), 9)) is not required to explain the delay in the observation of a Cr minimum near the grain boundaries.

The present model, consistent with experimental observations, predicts a delay in reaching a minimum interface chromium concentration at a small distance away from the carbide–matrix interface whilst maintaining the local equilibrium at the interface. It is also shown that the effect of intragranular precipitation on desensitisation cannot be neglected when considering large grain sizes.

## REFERENCES

- 1) D. E. Coates: *Metall. Trans.*, **3** (1972), 1203.
- 2) D. E. Coates: *Metall. Trans.*, **4** (1973), 1077.
- 3) C. Stawström and M. Hillert: *J. Iron Steel Inst.*, **207** (1969), 77.
- 4) G. S. Was and R. M. Kruger: *Acta Metall.*, **33** (1985), 841.
- 5) E. L. Hall and C. L. Briant: *Metall. Trans. A*, **15A** (1984), 793.
- 6) S. M. Bruemmer: *Corrosion*, **46** (1990), 698.
- 7) S. M. Bruemmer and L. A. Charlot: *Scr. Metall.*, **20** (1986), 1019.
- 8) H. Sahlaoui, H. Sidhom and J. Philibert: *Acta Mater.*, **50** (2002), 1383.
- 9) W. E. Mayo: *Mater. Sci. Eng. A*, **A232** (1997), 129.
- 10) J. W. Christian: *The Theory of Transformations in Metals and Alloys*, Pergamon Press, Oxford, (1965), 392.
- 11) J. Ågren: *J. Iron Steel Inst.*, **32** (1992), 291.
- 12) T. Åkermark: *Div. Phys. Met.*, **44** (1991), S-100.
- 13) J. S. Kirkaldy and D. J. Young: *Diffusion in the Condensed State*, Institute of Metals, London, (1987), 151.
- 14) MTDATA, National Physical Laboratory, Teddington, Middlesex, UK, (1989).
- 15) R. L. Fullman: *Acta Metall.*, **30** (1982), 1407.
- 16) R. Beltran, J. G. Maldonado, L. E. Murr and W. W. Fisher: *Acta Metall.*, **45** (1997), No. 10, 4351.
- 17) M. H. Lewis and B. Hattersley: *Acta Metall.*, **13** (1965), 1159.
- 18) G. E. Dieter: *Mechanical Metallurgy*, 3 ed., Mac Graw Hill, London, (1986), 176.